Asociación Argentina
de Mecánica Computacional

Mecánica Computacional Vol XXVII, págs. 1601-1618 (artículo completo)
Alberto Cardona, Mario Storti, Carlos Zuppa. (Eds.)
San Luis, Argentina, 10-13 Noviembre 2008

NUMERICAL SIMULATION OF PACKED BED HEAT REGENERATORS

César Nieto-Londoño [a]

[a] *Instituto de Energía y Termodinámica, Universidad Pontificia Bolivariana, Circular 1 No. 73-34 Medellín, Colombia, cesar.nieto@upb.edu.co, http://www.upb.edu.co/medellin*

Keywords: Packed bed, heat regenerator, finite volume method.

Abstract. The study of packed beds as heat regenerators under different thermal conditions is the main objective of the present work. A three equation model was used to study the thermal behavior of the system. For the thermal interaction between the fluid and the packed bed, two local thermal non-equilibrium equations were used. The velocity field was calculated with the Darcy-Brinkman-Forchheimer extended momentum equation. Steady and unsteady heating as well as radial porosity variation were considered in the model. The Finite Volume Method was employed to solve the above mentioned set of Partial Differential Equations (PDEs). Numerical results were compared with both our own experimental data and previous results reported by peers. Computational errors were typically in the range of 2 to 12%, depending on the conditions imposed to the model.

INTRODUCTION

Packed Bed Heat Regenerators (PBHR) and Heat Exchangers (HES) are used to recover energy from combustion gases. Their implementation may reduce fuel burning rate levels up to 50% and, as a result, decrease the emission of pollutants. Among the advantages of using HES, we can mention their capability of handling gases at temperatures between 1000 to 1300°C to increase the comburent temperature over 650°C. Consequently, an overall thermal efficiency of 30 to 40% can be obtained. However, HES are more susceptible to damage under abrasive or corrosive flow and their sizes are larger than those of PBHR for the same applications. Besides, PBHR can be used at temperatures as high as 1370°C, with an overall thermal efficiency from 75 to 95% (Baillargeon et al., 1998). These relative advantages have made PBHRs suitable for some industrial applications, despite the fact that they are in general more expensive than HES.

The up-to-date designing tools for PBHR are not developed enough to find optimal configurations and operation conditions. Moreover, PBHR thermal optimization were faced by experimental (Nijemeisland, 2001; Mejía et al., 2004), analytical (Whitaker, 1972) and numerical approximations (Logtenberg and Dixon, 1998; Greyvenstein, 2002; Greyvenstein and van Antwerpen, 2005). Latter approximations have shown several advantages over the others ones, due to the possibility to probe any kind of configurations and operation conditions, without wasting time, energy resources and raw materials, with a higher precision compared with experimental results. Mathematical models used in numerical analysis, requires enough comprehension of the transport phenomena associated to PBHR. This permit a good estimation of PBHR behavior associated to several conditions.

The aim of the present work is to show the implementation of the Finite Volume Method (FVM) for the numerical study of PBHR. Various operation conditions and physical configurations were studied. Validation of numerical results was made through comparison with our experimental data and previous results reported by peers. The steps to implement the FVM for the solution of PBHR governing equations are presented. Porosity variation in radial direction was into account in the mathematical model formulation. Steady and unsteady heat transfer conditions were considered in the numerical analysis.

1 SIMULATION OF PACKED BEDS

Many systems use packed beds to improve their operational conditions. Some examples includes chemical reactors, air compressors adsorbed dryers and heat regenerators. Numerical simulations of packed beds have been developed for the design and develop of this type of devices. Two kind of numerical approximations are used to study packed beds behavior: geometry model simulation of packed elements and porous media estimation. Among the first, both 2D and 3D models of packed elements are developed to estimate pressure, velocity, temperature and concentration fields in fluids inside packed beds (Logtenberg and Dixon, 1998; Nijemeisland, 2001; Calis et al., 2001; Nieto et al., 2004). Besides, interaction between packed elements and heat and mass transport process has been estimated. Results from these simulations have shown that packed elements design most conduces to reduce fluid flow resistance and maximize heat transfer area.

Commercial codes like Fluent, Ansys and CFX (Derkx and Dixon, 1996; Tobiś, 2000; Romkes et al. 2003; Landman and Greyvenstein, 2004) have been used to show its proficiency to describe characteristic transport phenomena of packed bed under almost any situation. High computational effort during preprocess (i.e. geometric model preparation, mesh grid design, boundary conditions implementation), and elevated solution times and

computational resources (i.e. high memory and processor load), are the principal drawbacks of commercial Computational Fluid Dynamics (CFD) simulations of packed beds.

Approximation to packed beds behavior through porous media models improves the use of computational resources during numerical simulations. In porous media approximation packed elements geometry is not modeled. Last condition reduces excessive preprocessing and solution times. Instead of model the geometry, the packed elements' fluid flow resistance is incorporated by porous distribution and sources terms associated with drag effects.

The porous distribution describes empty space between packed elements. Porosity distribution has the property to influence velocity and temperature fields (Whitaker, 1972; Tobiś, 2000; du Toit, 2002). The porosity distribution is function of the size and shape of the elements inside the container. Several works were developed to find mathematical models for describing packed beds porosity distribution as function of size and shape of elements (Nandakumar, 1999; Alazmi and Vafai, 2000; Sahimi, 2000; du Toit, 2002; Jiang, 2002), but just a few of them had been applied extensively (Mueller, 1991).

Mass, momentum and energy balances in PBHT conduce to partial differential equations based on control volume models. Sources terms like Forchheimer and Darcy (Nield and Bejan, 1999) are included into the momentum equation to consider inertial drag and draining through porous media effects, respectively. Viscous shear stress is considered by a diffusivity viscous term named Brinkman term.

Heat transfer forced convection in PBHR would be studied by means of two different models: Local Thermal Equilibrium (LTE) and Local Thermal Non Equilibrium (LTNE) (Vafai, 2002). The first one accounts thermal equilibrium between packed elements and combustion gases (both gases and elements have the same temperature). This simplification produces an energy equation in terms of gases and elements temperature. LTNE conduces to one energy equations for gases and one for elements, since non equilibrium between both phases is accepted. PBHR currently used in industrial applications has high Darcy numbers (Mejía, 2004). High Darcy numbers implies the rejection of equilibrium between packed bed phases (gases and elements), assuming valid the LTNE model which conduces to two energy equation for predicting temperature fields.

NOMENCLATURE

A	area [m^2]
a	packed bed specific area [m^{-1}]
B	momentum source term
c	specific heat at constant pressure [J/kg·K]
C_f	Forchheimer coefficient
d	diameter [m]
f	friction factor
F	convective mass flux per unit area [kg/s]
D	diffusion conductance [W/k]
h	convective heat transfer coefficient [$W/m^2 \cdot K$]
k	thermal conductivity [W/mK]
P	pressure [Pa]
T	temperature [K or °C]
t	time [s]
u	velocity component x direction [m/s]
v	velocity component y direction [m/s]
V	volume [m^3]
x	axial coordinate [m]
y	transversal coordinate [m]
b, c	porosity model coefficients
n	normal vector to surface

GREEK SYMBOLS

α	thermal diffusivity [m^2/s]
ε	porosity or empty space fraction
μ	dynamic viscosity [kg/m·s]
ρ	density [kg/m^3]

SUBINDICES

e,w,n,s	sides of integral control volume
eff	referenced to effective property
f	referenced to fluid phase
fs	referenced to fluid-solid interaction
fw	referenced to fluid-wall interaction
p	referenced to solids or packed particles
s	referenced to solid phase

2 MATHEMATICAL MODEL

The governing equations for porous media include the continuity (1), momentum (2)-(3) and energy balance (6)-(7). Its solution conduces to prediction of velocity, pressure and temperature fields of gases and elements into packed bed regenerator. The continuity, momentum and energy equation in 2D cartesian coordinates are as follows (Nield and Bejan, 1999; Vafai, 2002).

$$\frac{\partial(\varepsilon u)}{\partial x}+\frac{\partial(\varepsilon v)}{\partial y}=0 \tag{1}$$

$$\rho\left(\frac{\partial(\varepsilon u u)}{\partial x}+\frac{\partial(\varepsilon v u)}{\partial y}\right)=\mu\frac{\partial}{\partial x}\left(\frac{\partial(\varepsilon u)}{\partial x}\right)+\mu\frac{\partial}{\partial y}\left(\frac{\partial(\varepsilon u)}{\partial y}\right)-\varepsilon\frac{\partial P}{\partial x}-B_x u \tag{2}$$

$$\rho\left(\frac{\partial(\varepsilon u v)}{\partial x}+\frac{\partial(\varepsilon v v)}{\partial y}\right)=\mu\frac{\partial}{\partial x}\left(\frac{\partial(\varepsilon v)}{\partial x}\right)+\mu\frac{\partial}{\partial y}\left(\frac{\partial(\varepsilon v)}{\partial y}\right)-\frac{\partial(\varepsilon P)}{\partial y}-B_y u \tag{3}$$

The momentum balance equation is an extended formulation of Darcy-Brinkman-Forchheimer (Mejía, 2004). The source terms effects as well porosity distribution are considered to enhance mathematical model capabilities for describing PBHRs physical behavior. Source terms B_x (4) and B_y (5), for both momentum equations are as shown below. The first term on the right side is related to Darcy effect (viscous shear) while the second one is the Forchheimer term (fluid´s inertia).

$$B_x=\mu\frac{150(1-\varepsilon)^2}{\varepsilon^3 d_p^2}+\rho\frac{1.75(1-\varepsilon)}{\varepsilon^3 d_p}\cdot u \tag{4}$$

$$B_y=\mu\frac{150(1-\varepsilon)^2}{\varepsilon^3 d_p^2}+\rho\frac{1.75(1-\varepsilon)}{\varepsilon^3 d_p}\cdot v \tag{5}$$

The energy equations for elements (6) and gases (7) are deduced through LTNE formulation, which as was mentioned above, is the correct consideration for packed beds that are usually present in industrial heat regenerators due to the presence of higher Darcy numbers. Because porosity ε, is a function of direction perpendicular to the flow (y direction), its effect is considered through its inclusion into the mathematical model as is shown.

$$(1-\varepsilon)\frac{\partial(\rho_s T_s)}{\partial t}=\nabla\cdot\left(\frac{K_{s,eff}}{C_s}\nabla(T_s)\right)-\frac{h_{fs}a_{fs}}{C_s}\left(T_s-T_f\right) \tag{6}$$

$$\varepsilon\frac{\partial(\rho_f T_f)}{\partial t}+\nabla\cdot(\rho_f T_f\mathbf{u})=\nabla\cdot\left(\frac{K_{f,eff}}{C_f}\nabla(T_f)\right)+\frac{h_{fs}a_{fs}}{C_f}(T_s-T_f) \tag{7}$$

3 MODEL CONDITIONS

Well posed numerical problems need the definition of adequate boundary and initial conditions for fluid flow and heat transfer as well as property variation and mathematical and model simplifications. The fluid flow through the packed bed is defined laminar and incompressible. The first assumption is due to lower Reynolds numbers which indicate that viscous forces are higher than the inertial ones into the flow. The incompressibility of the gases is valid because the pressure gradient in the flow is small.

3.1 Boundary and initial conditions

Since time scale for heat transfer process is higher than that for momentum transport, time

dependent simulations are carry out just for energy equations. According to that, initial conditions must be defined for packed elements and fluids gases through all heat regenerator domains before the start of the warming up process. Neither heat transfer contact between packed elements nor conduction into them are considered. Moreover heat transfer by radiation between solids and gases is not included.

Both boundary and initial conditions must be defined to have a well mathematical established problem (see Figure 1). Constant velocity and temperature are at the inlet boundary. Boundary walls are employed and no slip velocity conditions and constant temperature are defined on that. At the outlet boundary the flow is considered fully developed for temperature and velocity fields, so temperature and velocity gradients in normal direction to boundary direction are properly defined. Moreover the fluid flow gases are exposed to atmospheric condition and then atmospheric pressure is defined at the outside boundary. Finally, due to flow and heat transfer symmetry, a symmetry condition is considered at the core of packed bed, to reduce computation effort.

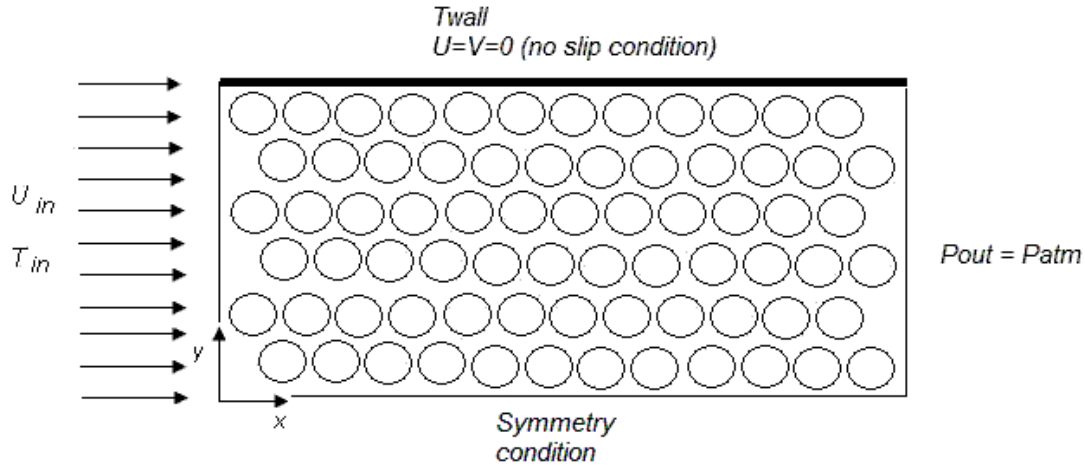

Figure 1. System scheme simplification

3.2 Porosity distribution model

Despite constant properties conditions are considered for packed elements and gases, the porosity distribution in the direction perpendicular to the flow is included by means of equation (8) (Bey and Eigenberger, 1997), which introduces an absorbing sinusoidal type profile for the porosity distribution as is suggested for several authors (Giese et al., 1998; Nandakumar et al., 1999; Taylor et al., 2002).

$$\varepsilon = \varepsilon_b \left[1 + b \cdot exp\left(\frac{-cy}{d_p}\right)\right] \tag{8}$$

Porosity distribution dominates fluid flow in packed beds. This variable is associated to packed elements shape and size. Porosity profiles present a maximum value near to the wall and converge to an average value next to packed core (Mueller, 1991). Higher velocities at the zone near the wall indicate the porosity profile effect on this area. Temperature and heat flux values are also associated to this geometrical distribution.

4 FINITE VOLUME DISCRETIZATION

The Finite Volume Method (FVM) is used to solve the PBHR governing equations model presented in the previous section. Volume integration of equations (1)-(7) is applied over mesh volumes presented in Figure 2. This process conduces to a set of linear equation for

each node in the mesh. In the present work the Conjugate Gradient Squared Method (CGSM) is applied to solve the system of linear equations obtained by the FVM application. The advantages of this method are associated with the precision of the physical balances (energy, mass and momentum) compared with other numerical methods.

Pressure and velocity fields are coupled by means of Semi-Implicit Method for Pressure-Linked Equations (SIMPLE) (Pantakar and Spalding, 1972). This means that a staggered grid (see Figure 2) is used to avoid underestimation of pressure contribution in momentum transport equations. The UPWIND discretization scheme is used for the momentum and energy convection term evaluation. This scheme has the advantage of predicting fluid flow direction, increasing the precision of the obtained numerical values (Versteeg and Malalasekera, 1995). The source terms in momentum (Darcy and Forchhaimmer effects (4)-(5)) and energy equations (heat convection between solid and gases due to h_{fs} (6)-(7)) are linearized according to Pantakar (1980) rules. Linearized terms are evaluated by an implicit method; this means that numerical results for velocity and temperature of last iteration are used to determine the current state of pressure, velocity and energy fields.

A four order degree Runge-Kutta method is used for transient solutions (Chapra and Canale, 2003). High order time steps (0,25 seconds) compared with other methods (semi-implicit, implicit, explicit, among others) were tested, but the Runge-Kutta application presented a better behavior during transient simulations. FVM implementation of the packed bed mathematical model is presented in the next sections. First, steady state equations are integrated by use of the SIMPLE method. Then, transient state integration is applied for the analysis of energy transport phenomena.

4.1 Momentum equations discretization

Momentum equation in *x* and *y* directions are integrated through respective volumes presented in Figure 2. In the x direction the integrated momentum equation is as follows:

$$\int\left(\frac{\partial}{\partial x}(\rho\varepsilon uu)+\frac{\partial}{\partial y}(\rho\varepsilon vu)\right)dV=\int\left(\frac{\partial}{\partial x}\left(\mu\frac{\partial}{\partial x}(\varepsilon u)\right)+\frac{\partial}{\partial y}\left(\mu\frac{\partial}{\partial y}(\varepsilon u)\right)\right)dV - \int\left(\varepsilon\frac{\partial P}{\partial x}\right)dV-\int(B_x u)dV \tag{9}$$

And for *y* direction, the momentum equation is:

$$\int\left(\frac{\partial}{\partial x}(\rho\varepsilon uv)+\frac{\partial}{\partial y}(\rho\varepsilon vv)\right)dV=\int\left(\frac{\partial}{\partial x}\left(\mu\frac{\partial}{\partial x}(\varepsilon v)\right)+\frac{\partial}{\partial y}\left(\mu\frac{\partial}{\partial y}(\varepsilon v)\right)\right)dV - \int\left(\varepsilon\frac{\partial P}{\partial y}\right)dV-\int(B_y v)dV \tag{10}$$

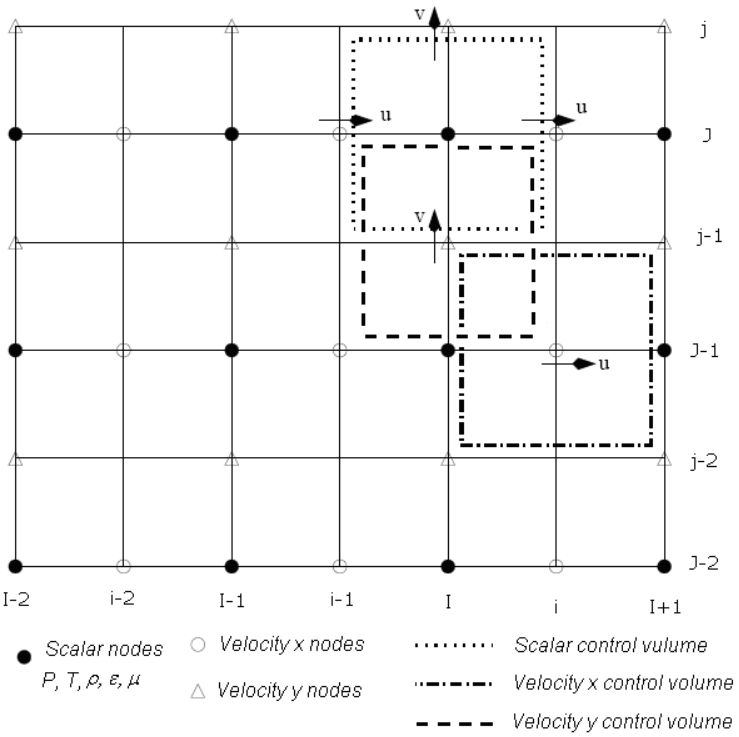

Figure 2. Finite volume meshes used for numerical integration of equations (1)-(7)

Application of divergence theorem over integrated terms conduces to equation (11) for *x* direction and equation (12) for *y* direction, in which volume integrals are transformed into surface integrals:

$$\int\left(\left(\vec{n}_x\cdot\rho\varepsilon uu\right)+\left(\vec{n}_y\cdot\rho\varepsilon vu\right)\right)dA=\int\left(\vec{n}_x\cdot\left(\mu\frac{\partial}{\partial y}(\varepsilon u)\right)+\vec{n}_y\cdot\left(\mu\frac{\partial}{\partial y}(\varepsilon u)\right)\right)dA \\ -\int\vec{n}_x\cdot(\varepsilon P)dA-\int(B_x u)dV \tag{11}$$

$$\int\left(\left(\vec{n}_x\cdot\rho\varepsilon uv\right)+\left(\vec{n}_y\cdot\rho\varepsilon vv\right)\right)dA=\int\left(\vec{n}_x\cdot\left(\mu\frac{\partial}{\partial y}(\varepsilon v)\right)+\vec{n}_y\cdot\left(\mu\frac{\partial}{\partial y}(\varepsilon v)\right)\right)dA \\ -\int\vec{n}_y\cdot(\varepsilon P)dA-\int(B_y v)dV \tag{12}$$

The balances of convective and diffusion momentum transport in *x* direction through each face of the volume shown in Figure 2 are presented in (13) and (14):

$$\int\left(\left(\vec{n}_x\cdot\rho\varepsilon uu\right)+\left(\vec{n}_y\cdot\rho\varepsilon vu\right)\right)dA=(\rho\varepsilon uu)_e-(\rho\varepsilon uu)_w+(\rho\varepsilon vu)_n-(\rho\varepsilon vu)_s \tag{13}$$

$$\int\left(\vec{n}_x\cdot\left(\mu\frac{\partial}{\partial x}(\varepsilon u)\right)+\vec{n}_y\cdot\left(\mu\frac{\partial}{\partial y}(\varepsilon u)\right)\right)dA= \\ \left(\mu\frac{\partial}{\partial x}(\varepsilon u)\right)_e-\left(\mu\frac{\partial}{\partial x}(\varepsilon u)\right)_w+\left(\mu\frac{\partial}{\partial y}(\varepsilon u)\right)_n-\left(\mu\frac{\partial}{\partial y}(\varepsilon u)\right)_s \tag{14}$$

Similar expressions are obtained for the convective (15) and diffusion (16) momentum transported in *y* direction:

$$\int\left(\left(\vec{n}_x\cdot\rho\varepsilon uv\right)+\left(\vec{n}_y\cdot\rho\varepsilon vv\right)\right)dA=\left(\rho\varepsilon uv\right)_e-\left(\rho\varepsilon uv\right)_w+\left(\rho\varepsilon vv\right)_n-\left(\rho\varepsilon vv\right)_s \tag{15}$$

$$\int\left(\vec{n}_x\cdot\left(\mu\frac{\partial}{\partial x}(\varepsilon v)\right)+\vec{n}_y\cdot\left(\mu\frac{\partial}{\partial y}(\varepsilon v)\right)\right)dA= \left(\mu\frac{\partial}{\partial x}(\varepsilon v)\right)_e-\left(\mu\frac{\partial}{\partial x}(\varepsilon v)\right)_w+\left(\mu\frac{\partial}{\partial y}(\varepsilon v)\right)_n-\left(\mu\frac{\partial}{\partial y}(\varepsilon v)\right)_s \tag{16}$$

Since density and viscosity are considered constant all over fluid domain they step out the integrated terms and are evaluated at the center of the scalar volume in the mesh. Besides, porosity variates in *y* direction, so it is evaluated by a center diference scheme as follows. Convective mass flux per unit area *F* and diffusion conductance *D*, are define to simplify linear equation system assambly. For each balance direction, previous variables are defined as follows.

In *x* direction:

$$D_e=D_w=\frac{\mu}{\Delta x}\qquad D_s=D_n=\frac{\mu}{\Delta y}$$

$$F_e=\left(\rho\varepsilon u\right)_e=\left(\rho\varepsilon\right)_{I,J}\frac{u_{i,J}+u_{i+1,J}}{2}$$

$$F_w=\left(\rho\varepsilon u\right)_w=\left(\rho\varepsilon\right)_{I,J}\frac{u_{i-1,J}+u_{i,J}}{2} \tag{17}$$

$$F_n=\left(\rho\varepsilon v\right)_n=\left(\rho\right)_{I,J}\frac{\varepsilon_{I,J}+\varepsilon_{I,J+1}}{2}\frac{v_{I-1,j+1}+v_{I,j+1}}{2}$$

$$F_s=\left(\rho\varepsilon v\right)_s=\left(\rho\right)_{I,J}\frac{\varepsilon_{I,J}+\varepsilon_{I,J-1}}{2}\frac{v_{I-1,j-1}+v_{I,j-1}}{2}$$

In *y* direction:

$$D_e=D_w=\frac{\mu}{\Delta x}\qquad D_n=D_n=\frac{\mu}{\Delta y}$$

$$F_e=\left(\rho\varepsilon u\right)_e=\left(\rho\varepsilon\right)_{I,J}\frac{u_{i+1,J}+u_{i+1,J-1}}{2}$$

$$F_w=\left(\rho\varepsilon u\right)_w=\left(\rho\varepsilon\right)_{I,J}\frac{u_{i,J}+u_{i,J-1}}{2} \tag{18}$$

$$F_n=\left(\rho\varepsilon v\right)_n=\left(\rho\varepsilon\right)_{I,J}\frac{v_{I,j}+v_{I,j+1}}{2}$$

$$F_s=\left(\rho\varepsilon v\right)_s=\left(\rho\varepsilon\right)_{I,J-1}\frac{v_{I,j}+v_{I,j-1}}{2}$$

Finally, algebraic equations (19)-(20) for each node in mesh are assembled after introduction of terms (17) and (18) in equations (13)-(14) and (15)-(16), respectively. The set of algebraic linear equations is then solved to obtain numerical values of velocity and pressure fields.

In *x* direction, the set of linear equations is as follows:

(19)

and, in *y* direction the set of equations is as follows:

$$a_{I,j}v_{I,j} = \sum a_{nb}u_{nb} + \left[(\varepsilon P)_{I,J-1} - (\varepsilon P)_{I,J}\right]A_{I,j} + b_{I,j} \tag{20}$$

where, for both (19) and (20):

$$\sum a_{nb}u_{nb} = a_{i-1,J}u_{i-1,J} + a_{i+1,J}u_{i+1,J} + a_{I,j+1}u_{I,j+1} + a_{I,j-1}u_{I,j-1}$$

$$a_{i-1,J} = D_w + \max(F_w, 0)$$

$$a_{i+1,J} = D_e + \max(0, -F_e).$$

$$a_{I,j+1} = D_n + \max(F_n, 0)$$

$$a_{I,j-1} = D_s + \max(0, -F_s).$$

$$a_{i,J} = a_{i-1,J} + a_{i+1,J} + a_{I,j+1} + a_{I,j-1} + \Delta F - S_p$$

$$\Delta F = F_e - F_w + F_n - F_s$$

4.2 Linearization of sources terms

Source terms (4)-(7) and pressures are integrated over the scalar volume mesh in Figure 2. Source terms are linearized as follows, keeping in mind that coefficient terms in linear equations must be positives to satisfy the requirements for boundedness (Versteeg and Malalasekera, 1995):

$$\begin{aligned} \int (B_x u)dV &= B_x u_{i,J}\Delta V = B_x u_{i,J}\Delta x = b_{i,J} \\ \int (B_y v)dV &= B_y v_{I,j}\Delta V = B_y v_{I,j}\Delta y = b_{I,j} \end{aligned} \tag{21}$$

$$\begin{aligned} b_{i,J} &= \left(300\mu\frac{(1-\varepsilon)^2}{\varepsilon^2 {d_p}^2} + 3.5\rho\frac{1-\varepsilon}{\varepsilon^2 d_p}u^*_{i,J}\right)u^*_{i,J}\Delta x \\ b_{I,j} &= \left(300\mu\frac{(1-\varepsilon)^2}{\varepsilon^2 {d_p}^2} + 3.5\rho\frac{1-\varepsilon}{\varepsilon^2 d_p}v^*_{I,j}\right)v^*_{I,j}\Delta y \end{aligned} \tag{22}$$

where *u** and *v** means last iteration values. The pressure gradient in both momentum equations is integrated as is presented in (23), where pressure values are evaluated at scalar mesh nodes, as is expected due to staggered grid implementation.

$$\begin{aligned} \int \varepsilon\frac{\partial P}{\partial x}dV &= \int \vec{n}\cdot(\varepsilon P)dA = (\varepsilon PA)_e - (\varepsilon PA)_w = \varepsilon_{I,J}\left(P_{I,J} - P_{I-1,J}\right) \\ \int \varepsilon\frac{\partial P}{\partial y}dV &= \int \vec{n}\cdot(\varepsilon P)dA = (\varepsilon PA)_n - (\varepsilon PA)_s = \left(\varepsilon_{I,J}P_{I,J} - \varepsilon_{I,J-1}P_{I,J-1}\right) \end{aligned} \tag{23}$$

4.3 Energy equations integration for steady state

Steady state energy equations (6) and (7) are integrated over scalar volumes presented in Figure 2. Integration of energy equation for solids is as follows:

(24)

Applying the divergence theorem, the first volume integral term transforms into a surface one and then, Eq. (24) becomes:

$$\int_A \dot{n} \cdot \left(\frac{K_{s,eff}}{C_s}\nabla T\right) dA - \int_{VC} \frac{h_{fs}a_{fs}}{C_s}\left(T^s - T^f\right)dV = 0 \tag{25}$$

Finally:

$$\begin{aligned}&\left(\frac{K_{s,eff}}{C_s}\frac{\partial T}{\partial x}A\right)_e \left(\frac{K_{s,eff}}{C_s}\frac{\partial T}{\partial x}A\right)_w + \left(\frac{K_{s,eff}}{C_s}\frac{\partial T}{\partial y}A\right)_n \\ &-\left(\frac{K_{s,eff}}{C_s}\frac{\partial T}{\partial y}A\right)_s - \frac{h_{fs}a_{fs}}{C_s}\left(T^s_{I,J} - T^f_{I,J}\right)\Delta V = 0\end{aligned} \tag{26}$$

The steady state energy equations for fluid phase, is also integrated over the scalar volume; the integrated equation is as follows:

$$\int_{VC} \nabla \cdot \left(\rho_f T_f \vec{u}\right)dV = \int_{VC} \nabla \cdot \left(\frac{k_{f,eff}}{c_{p,f}}\nabla T\right)dV + \int_{VC} \frac{h_{fs}a_{fs}}{c_{p,f}}\left(T^s - T^f\right)dV \tag{27}$$

Applying the divergence theorem to control volume integrals in Eq. (27), it becomes in:

$$\int_A \vec{n} \cdot \left(\rho_f T_f \vec{u}\right)dA = \int_{VC} \vec{n} \cdot \left(\frac{k_{f,eff}}{c_{p,f}}\nabla T\right)dA + \int_{VC} \frac{h_{fs}a_{fs}}{c_{p,f}}\left(T^s - T^f\right)dV \tag{28}$$

Finally, integrated energy equation for fluid phase in packed bed is as follows:

$$\begin{aligned}\left(\rho_f u T_f A\right)_e - \left(\rho_f u T_f A\right)_w + \left(\rho_f v T_f A\right)_n - \left(\rho_f v T_f A\right)_s &= \left(\frac{k_{f,eff}}{c_{p,f}}A\frac{\partial T}{\partial x}\right)_e - \left(\frac{k_{f,eff}}{c_{p,f}}A\frac{\partial T}{\partial x}\right)_w \\ + \left(\frac{k_{f,eff}}{c_{p,f}}A\frac{\partial T}{\partial y}\right)_n - \left(\frac{k_{f,eff}}{c_{p,f}}A\frac{\partial T}{\partial y}\right)_s &+ \frac{h_{fs}a_{fs}}{c_{p,f}}\Delta V\left(T^s_P - T^f_P\right)\end{aligned} \tag{29}$$

5 RESULTS AND ANALYSIS

Results from numerical simulations of PBHR are presented below. A first validation of results is made by reproduction of some literature reported results. Then an experimental validation is carried out by comparison with values obtained in a packed bank test device. Finally several packed bed configurations are evaluated; geometric and operational conditions selection are considered to analyze their effects over PBHR's behavior.

5.1 Validation of numerical results

As first stage, numerical results obtained through finite volume solution for packed bed governing equations are compared with Duprat and López's (2001) work. Values of pressure loss and thermal efficiency are compared for different packed elements diameter, heat regenerators length and cycle time regeneration.

These results are used to determine the adequate grid size and time step effect over numerical results. Results for different mesh densities are used for governing equations solution. Thermal efficiency and pressure loss values are compared for different meshes. It is obvious that an increase in mesh volumes conduces to a decrease in relative errors. With the

aim of improving the use of hardware resources, keeping the simulation time small and the accuracy of results high, a 60 by 60 volumes mesh is selected as the best one (see Figure 3). Results in Figure 4 are for 95% thermal efficiency and those in Figure 5 are for pressure loss through packed bed for different heat regenerator longitude and elements diameter. Both, thermal efficiency and pressure loss results present minimal discrepancy (less than 1% for thermal efficiency and 10% for pressure loss) with the values reported by peers (Duprat and López, 2001).

The simulation time is in the 138 (steady state solutions) to 600 seconds range (transient state solutions) while the numerical error is 1,4 % for thermal efficiency and 17 % for pressure loss. The latter is considered as an acceptable error if it is compared with traditional results achieved by Ergun's equation which are over 50%.

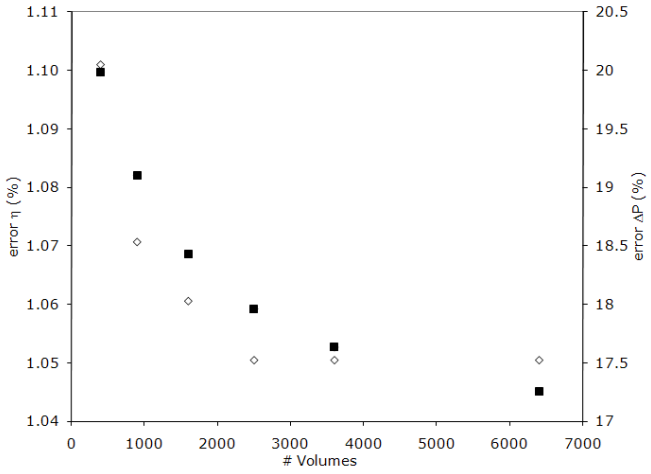

Figure 3. Analysis of solution mesh independence: ■ error ΔP, ◊ error η.

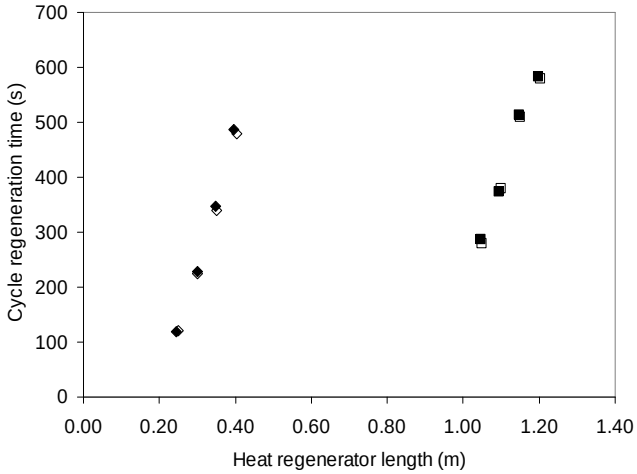

Figure 4. Cycle regeneration time for 95 % thermal efficiency and $\dot{m}$ = 30 kg/s. Packed bed of spheres: ◊ d_p = 1.5 mm, □ d_p = 5 mm, ■ d_p = 1.5 mm, ◆ d_p = 5 mm. (Duprat and López, 2001).

Model validation was also carried out by comparison between numerical and experimental results. Temperatures measured in an experimental device designed for the study of PBHR (Agudelo et al, 2004) were compared with computed values at different locations along the PBHR length. Figure 6 show the numerical and experimental time temperature evolution at three longitudinal positions in the packed bed. Differences between numerical results and experimental values are associated to mathematical model simplification and used measurement devices.

Nevertheless, it can be concluded that acceptable results of PBHR under stable and unstable conditions are obtained.

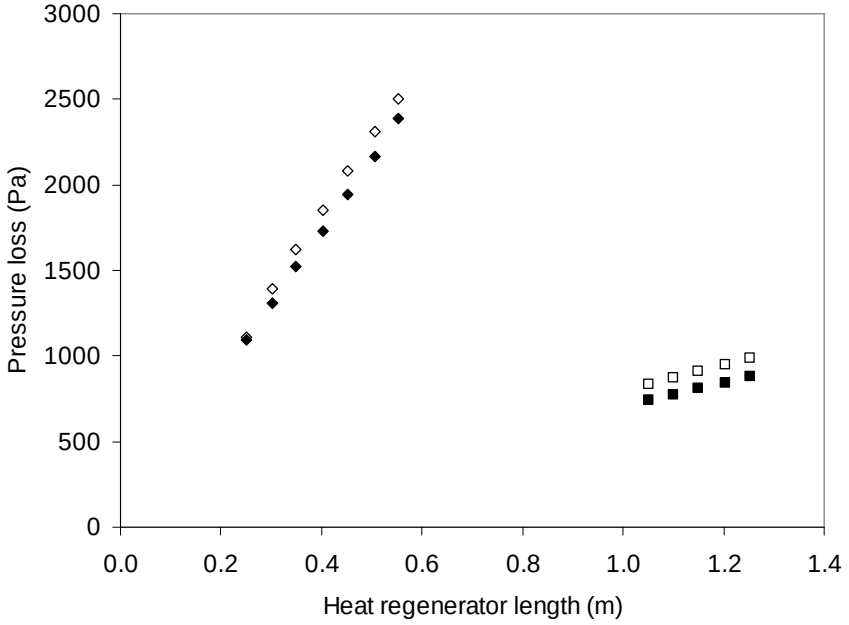

Figure 5. Pressure loss variation as function of packed bed length. $\dot{m}$ = 30 kg/s. Packed bed of spheres: ◊ dp = 1.5 mm, □ dp = 5 mm, ■ dp = 1.5 mm, ◆ dp = 5 mm. (Duprat and López, 2001).

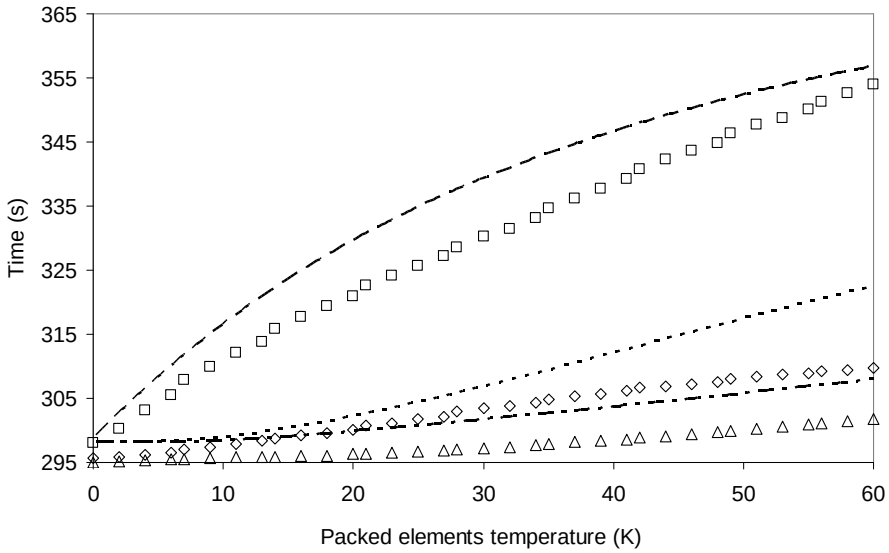

Figure 6. Packed elements time dependent temperature profiles. Spheres, dp =3/8", D = 0.082 m, L = 0.25 m, u = 1.66 m/s. Numerical simulation results: -- x_1 = 0.03 m, ····· x_2 = 0.09 m, -·- x_3 = 0.15 m. Experimental values: □ x_1 = 0.03 m, ◊ x_2 = 0.09 m, □ x_3 = 0.15 m.

5.2 Numerical characterization of PBHR

Since PBHR numerical model has been validated through experimental and literature comparison, it is possible to analyze PBHR behavior under different operational conditions. Packed bed diameter and length as well as material and diameter of packed elements have been changed to study their influences on PBHR behavior through thermal efficiency and pressures loss evaluation. In Figure 7 PBHR diameter effect over pressure loss is plotted. As packed bed regenerator diameter tends to increase the fluid velocity would be reduced as well the pressure

loss for the same element diameter and mass flow.

On the other hand, PBHR length variation increases the thermal efficiency of systems due to the extra heat transfer area. Despite of that, a higher pressure loss is present in the PBHR and then, more extra work must be done to move the combustion gases through the packed bed. Results for different PBHR lengths are plotted in Figure 8 and Figure 9. Moreover, is possible to conclude from results that PBHR thermal inefficiency increase at higher cycle regeneration times.

In contrast, a decrease in packed elements diameter conduces to higher heat transfer areas and higher thermal efficiencies, as well higher pressures loss and regeneration cycle times. Higher pressure losses are due to an increase in the contact fluid area which increases the drag force as well residence time for gases in the packed bed. The above mentioned effects are plotted in Figure 10 and Figure 11.

PBHR use metallic and ceramic elements to recover waste energy. Metallic elements produce shorter regeneration cycles, and more variations into gases conditions which affect overall regeneration process. In contrast, less thermal diffusive materials like ceramics conduce to more stable regeneration cycles (see Figure 12)

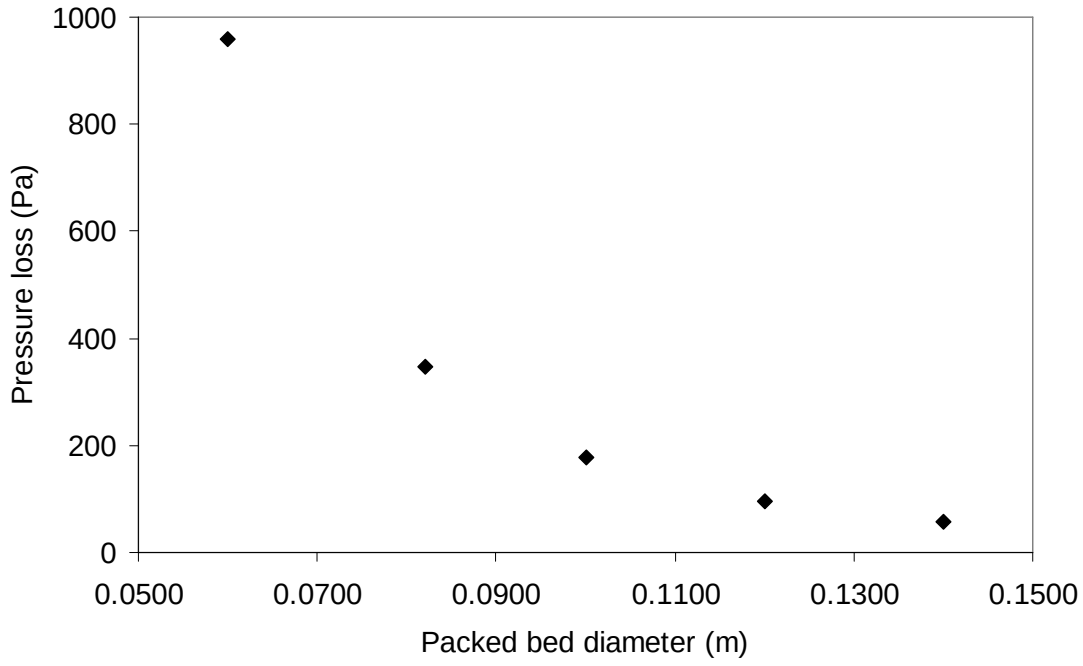

Figure 7. Pressure loss variation as function of packed bed diameter. Thermal efficiency 95 %. Velocity: 1.66 m/s.

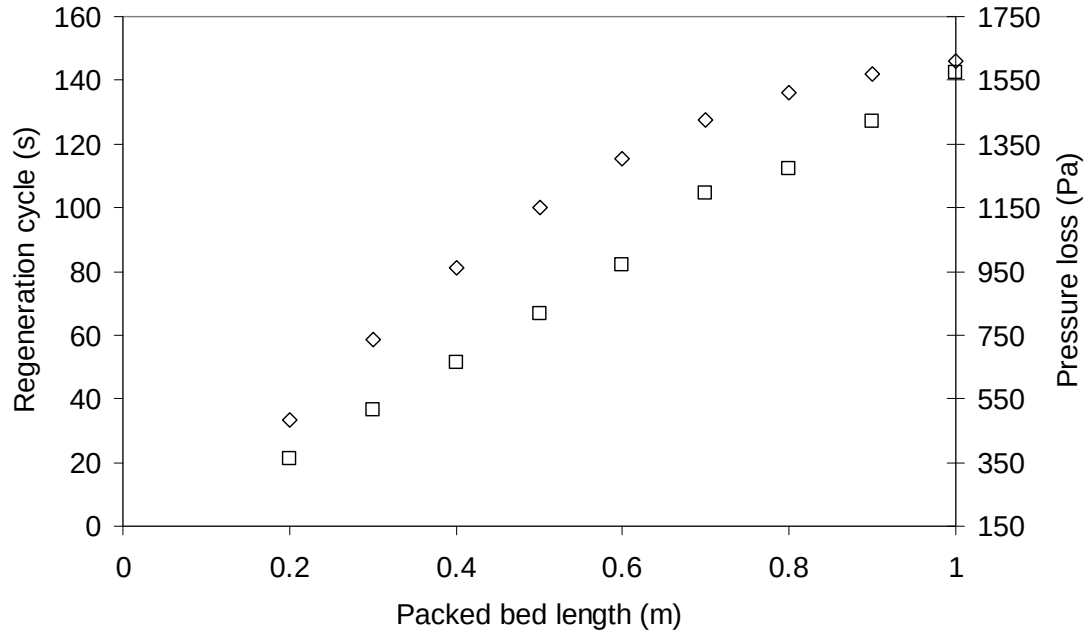

Figure 8. Regeneration cycle variation and pressure loss as length as function of PBHR length. Thermal efficiency 95 %. Velocity: 1.66 m/s. ◊ Regeneration cycle. □ Pressure loss.

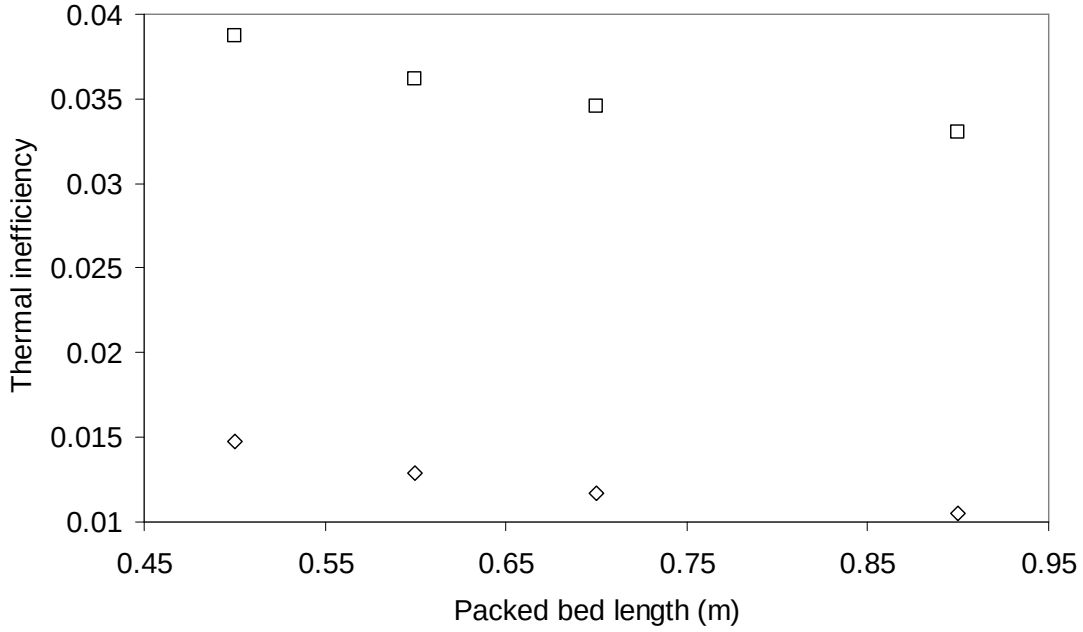

Figure 9. Thermal inefficiency as function of packed bed length and regeneration cycle. Velocity: 1.66 m/s. ◊ Regeneration cycle duration 10 seconds, □ Regeneration cycle time 60 seconds**.**

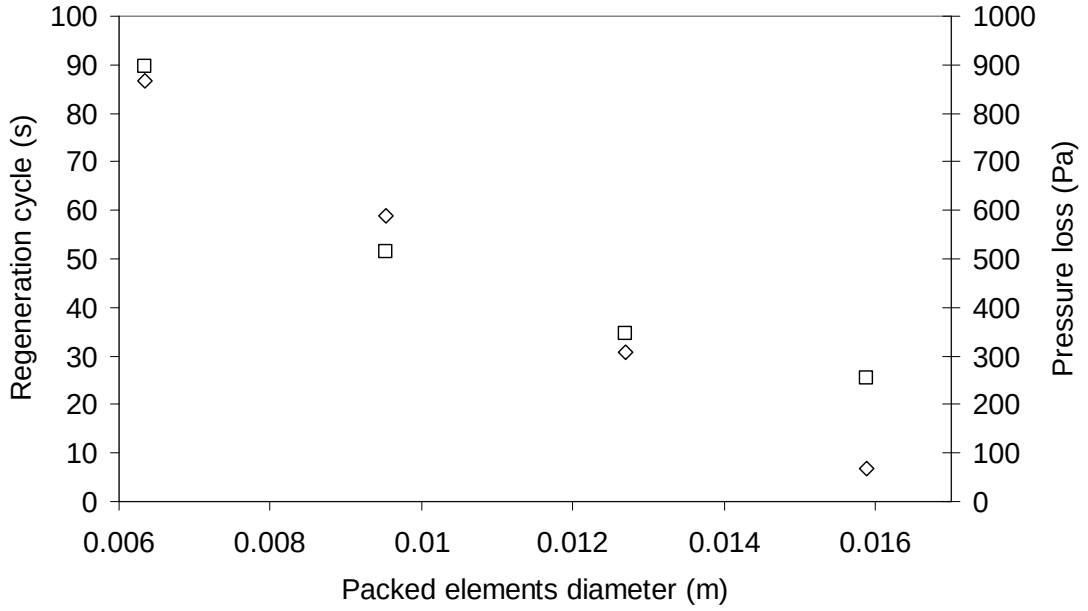

Figure 10. Regeneration cycle variation and pressure loss as function of elements diameter. Thermal efficiency 95 %. Velocity: 1.66 m/s. Regeneration cycle ◊. Pressure loss □

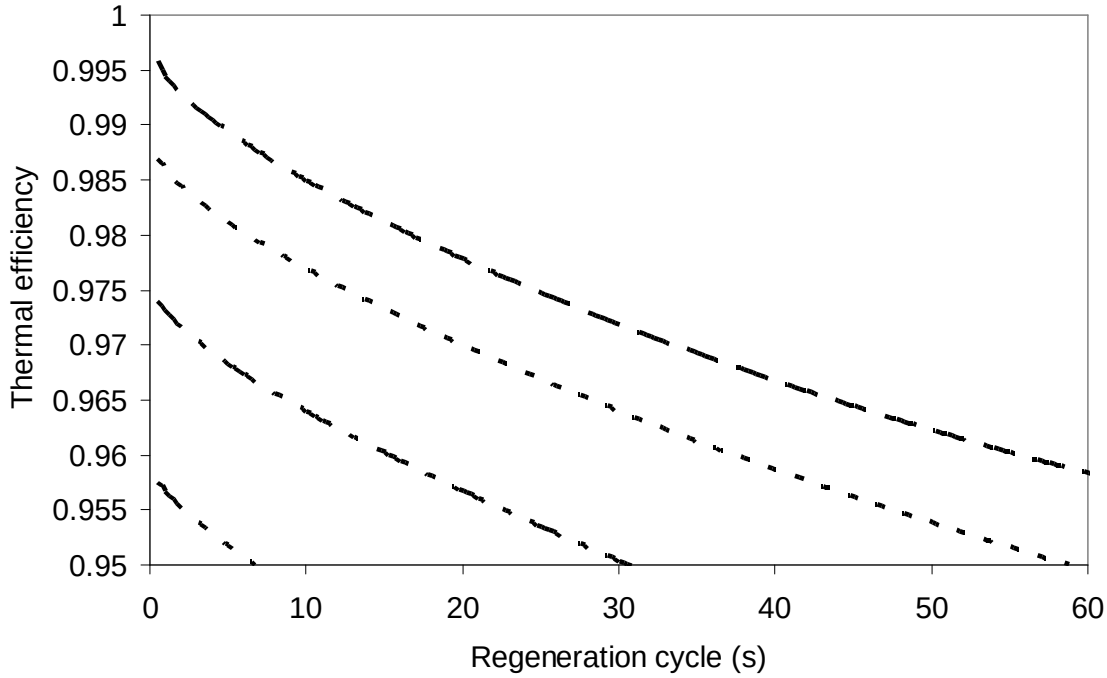

Figure 11. Thermal efficiency as function of regeneration cycle duration and elements size. – – dp = 6.35 mm; ····· dp = 9.525 mm; –·– dp = 12.7 mm; –··– dp = 15.875 mm

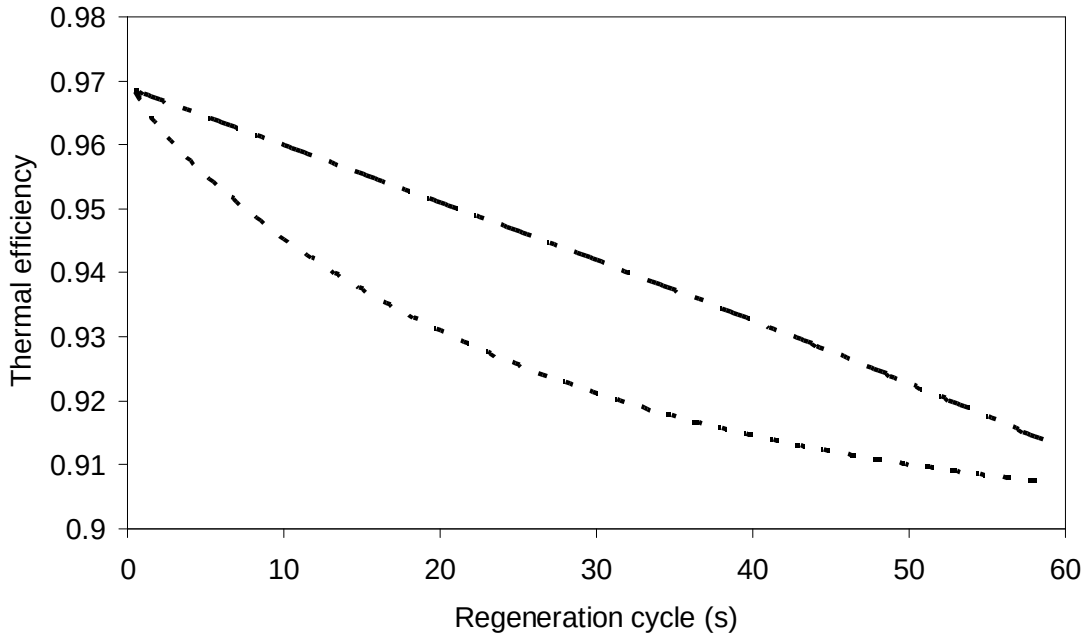

Figure 12. Thermal efficiency variation as function of packed bed material. -·- Ceramic elements $\alpha = 12.07 \times 10^{-8}$ m^2/s; -- Aluminum elements $\alpha = 68.19 \times 10^{-6}$ m^2/s

6 CONCLUSIONS

In the present work the finite volume method was used to solve governing equation of PBHR. From the numerical simulation and its validation, it is possible conclude that:

- Results obtained through finite volume application have shown agreement with experimental and literature results used for its validation. Besides, the study of steady and unsteady PBHR conditions was accurate enough to establish PBHR behavior under several conditions and configurations.
- Moreover, finite volume solution of PBHR improves solution time and computational resources. Those results are important for design and optimization process because bring the opportunity of evaluating several operation conditions with appropriate computational resources and with sufficient predicted accuracy.
- Porosity distribution is a geometric variable fundamental for the analysis of PBHR with porous media governing equation models. The consideration of porosity variation through the packed bed increase reliability of results achieved by numerical analysis.
- Finally it is possible to conclude that heat and momentum transfer process has an inverse interaction, since as high thermal efficiencies are achieved due by increasing the heat transfer area higher work also must be compensate for higher pressure losses.

7 ACKNOWLEDGMENTS

Financial support from the Colombian Institute of Science and Technology – Colciencias- (Project 1115-05-16053) is gratefully acknowledged. Also the Universidad de Antioquia, is gratefully acknowledged for their financial support during my master degree's fellowship in this academic institution.

REFERENCES

Agudelo J.R., Mejía, R., Villa L.C. and Nieto C., Montaje Experimental para Recuperadores de Calor. *En memorias de: Primer congreso internacional sobre uso racional y eficiente de la energía*, 2004.

Alazmi, B. and Vafai, K., Analysis of Variants Within Porous Media Transport Models. *Journal of Heat Transfer*, 122, 303-326, 2000.

Baillargeon, P., Leclerc, D. and Zahar, H., Guide to Energy Efficiency in Aluminium Smelter. Consultado en junio 20, 2006 en *http://www.oee.rncan.gc.ca/Publications/industrial/M27-01-1115E/introduction.cfm?text=N&printview=N*, 2006.

Bey, O. and Eigenberger, G., Fluid Flow Through Catalyst Filled Tubes. *Chemical Engineering Science*, 52-8, 1365-1376, 1997.

Calis, H. P. A., Nijenhuis, J., Paikert, B. C., Dautzenberg, F. M., van den Bleek, C. M., CFD modeling and experimental validation of pressure drop and flow profile in a novel structures catalytic reactor packing. *Chemical Engineering Science*, 56, 1713, 2001.

Chapra, S. and Canale, R., *Métodos numéricos para ingenieros*. Mc. Graw-Hill, 2003.

Derkx, O.R. and Dixon, A.G., Determination of the fixed bed wall heat transfer. *Numerical Heat Transfer-Part A*, 29, 777-794, 1996.

du Toit, C.G., The numerical determination of the variation in the porosity of the pebble- bed core. En *www.iaea.org/inis/aws/htgr/fulltext/htr2002_p08.pdf*, 2002.

Duprat, F., and López, G., Comparison of performance of heat regenerators: Relation between heat transfer efficiency and pressure drop. *International Journal of Energy Research*, 25, 319-329, 2001.

Giese, M., Rottschäfer K. and VORTMEYER D., Measured and Modeled Superficial Flow Profiles in Packed Beds with Liquid Flow. *Aiche Journal*, 44, 484-490, 1998.

Greyvenstein, G.P. An implicit method for the analysis of transient flows in pipe networks. *International Journal for Numerical Methods in Engineering*, 53, 1127-1143, 2002.

Greyvenstein, G.P. and van Antwerpen, H.J., A Finite Volume-Based Network Method for the Prediction of Heat, Mass And Momentum Transfer in a Pebble Bed Reactor. *2nd International Topical Meeting on HIGH TEMPERATURE REACTOR TECHNOLOGY*, 2005.

Landman, W.A. and Greyvenstein, G.P., Dynamic Systems CFD Simulation Code for the Modeling of HTGR Power Plants. *2nd International Topical Meeting on HIGH TEMPERATURE REACTOR TECHNOLOGY*, 2004.

Logtenberg, S.A. and Dixon, A.G., Computational Fluid Dynamics Studies of Fixed Bed Heat Transfer. *Chemical Engineering Science*, 39-18, 3931-3947, 1998.

Mejía, R., Modelamiento de la convección forzada transitoria en lechos empacados (Tesis de Maestría en Ingeniería Energética, Universidad de Antioquia), 2004.

Mejía, R., Agudelo, J., Nieto, C., Villa L., Unsteady forced convection in packed beds (computational and experimental analysis). *ASME International Mechanical Engineering Congress And Rd&D Expo*, 2004.

Muller, G. Prediction of Radial Porosity Distributions in Randomly Packed Fixed beds of Uniformly Sized Spheres in Cylindrical Containers. *Chemical Engineering Science*, 46, 706-708, 1991.

Nandakumar, K., Yiqiang Shu, Chuang, K. T., Predicting geometrical properties of random packed beds from computer simulation. *AIChE Journal*, 45, 2286-2297, 1999.

Nield, D.A. and Bejan, A. Convection in Porous Media. *Springer*, 1999.

Nieto, C., Mejía, R., Agudelo, J., Dinámica de fluidos computacional aplicada al estudio de regeneradores térmicos. *DYNA*, 143, 81-93, 2004.

Nijemeisland, M., Verification studies of computational fluid dynamics in fixed bed heat transfer (Master of Science Thesis in Chemical Engineering, Worcester Polytechnic Institute), 2001.

Patankar, S.V. and Spalding, D.B. A Calculation Procedure for Heat, Mass and Momentum Transfer in Three-Dimensional Parabolic Flows. *Int. J. Heat Mass Transfer*. 15, 1787-1806, 1972.

Patankar, S.V. Numerical Heat Transfer and Fluid Flow. *Taylor-Francis*, 1980.

Romkes, S. J. P., Dautzenberg, F. M., van den Bleek, C. M., and. Calis H. P. A., CFD modelling and experimental validation of particle-to-fluid mass and heat transfer in a packed bed at very lo chhanel to particle diameter ratio. *Chemical Engineering Journal*, 96, 3-13, 2003

Rousseau, P.G., du Toit, C.G. and Landman, W.A., Validation of a Transient Thermal-Fluid Systems CFD Model for a Packed Bed High Temperature Gas-Cooled Nuclear Reactor. *2nd International Topical Meeting on HIGH TEMPERATURE REACTOR TECHNOLOGY*, 2004.

Sahimi, M. Characterization of geology of, and flow and transport in, field-scale porous media. Application of fractal and percolation concepts. *Handbook of porous media*, Marcel Dekker; 113-170, 2000.

Taylor, K., Smith, A.G., Ross, S. and Smith, M., The prediction of pressure drop and flow distribution in packed bed filters. *http://www.cfd.com.au/cfd_conf99/Conf99_papers/071TAYL.pdf*, 1998

Tobiś, J., Influence of bed geometry on its frictional resistance under turbulent flow conditions. *Chemical Engineering Science*, 55, 5359, 2000.

Vafai, K., *Handbook of Porous Media*. Marcel Dekker, 2000.

Versteeg H. K. and W. Malalasekera., *An introduction to computational fluid dynamics: The finite volume method*. Longman Scientific & Technical, 1995.

Whitaker, S., Forced convection heat transfer correlations for flow in pipes, past flat plates, single cylinders, single spheres, and for flow in packed beds and tube bundles. *AIChE Journal*, 18, 361-371, 1972.

Y. Jiang, M. R. Khadilkar, M. H. Al-Dahhan and M. P. Dudokovic., CFD of multiphase flow in packed bed reactor: I. k-Fluid modeling issues. *AIChE Journal*, 48, 701, 2002.